Edward L. Ginzton Laboratory
Stanford University
Stanford, California 94305-4085

A
Final Report
For

An
All-Solid-State
Chirped Source
for
Coherent Optical Radar

ONR Contract Number N00014-88-K-0701

Principal Investigator
Robert L. Byer, Professor of Applied Physics
Dean of Research
Stanford University
Stanford, California 94305-4085
(415) 723-0226

March 15, 1992

Edward L. Ginzton Laboratory
Stanford University
Stanford, California 94305-4085

A Final Report For An All-Solid-State Chirped Source for Coherent Optical Radar

ONR Contract Number N00014-88-K-0701

Principal Investigator
Robert L. Byer, Professor of Applied Physics
Dean of Research
Stanford University
Stanford, California 94305-4085
(415) 723-0226

March 15, 1992

Abstract

A low-noise, high-power, single-frequency, solid-state laser harmonically converted to the green is required to pump a single-frequency, singly-resonant, chirped, optical parametric oscillator. As work toward this new frequency agile source we have built and injection locked an 18 watt Nd:YAG slave laser with a 40 mW master laser to produce single frequency operation, generated 6.5 watts of 532 nm radiation at 36% efficiency by resonant second harmonic generation, and measured spectral and spatial mode characteristics of this laser. Toward an all-solid-state version of this laser we have designed a diode-laser-pumped Nd:YAG laser. All subsystems of this laser have been built and tested and the final construction of the laser is currently underway. In addition, we have built both a pulsed singly resonant optical parametric oscillator, and a low threshold cw doubly resonant optical parametric oscillator that operated at 80% conversion efficiency in a single axial mode.

Introduction

Recent progress under the Office of Naval Research contract ONR N00014-88-K-0701, "An All-Solid-State Chirped Source for Coherent Optical Radar" is described here and in the publications and dissertations resulting from this program listed below and contained in the Appendix. We report seven principle accomplishments: 1) demonstration of an 18-watt, single-frequency, injection-locked, TEM_{00}, Nd:YAG laser, [1] 2) measurement of the phase fidelity of this regenerative amplifier and the frequency, and intensity noise of the injection locked laser, 3) conversion of the output of this laser to 6.5 watts of single-frequency, TEM_{00}, green radiation at 532 nm by resonant second harmonic generation, [2], 4) the of measurement of the spatial mode characteristics of this lasers [2] and its second harmonic, 5) progress toward a 13-watt, single-frequency, diode-laser-pumped, solid-state laser, 6) the construction and testing of a pulsed parametric oscillator,[3] and 7) the construction of a cw doubly resonant parametric oscillator and the use of this 80% efficient device for the generation of squeezed states.[4] This report is divided into eleven sections. Seven sections describe each of the accomplishments listed above, two sections list the publications and dissertations resulting from this program, a section listing the personnel supported and a conclusion.

18-W injection locked lamp-pumped Antares laser

The single-frequency, singly-resonant, parametric oscillator, pump laser requirements include: low frequency noise, low amplitude noise, good spatial mode quality and high output power. The approach we have selected to meet these requirements is to use injection locking where the stability of a low power master oscillator controls the spectral characteristics of the high power slave oscillator. The low power master is extremely stable and is described in reference [5] which describes frequency stabilization of diode-laser-pumped solid state lasers. The frequency noise of the low power master oscillator is impressed on the high power slave oscillator by injection locking. The slave laser acts like a regenerative amplifier and reproduces the spectral properties of the master at high power.[6]

Injection locking

In injection locking, the phase of a high power oscillator, the slave, is locked to the phase of a low power oscillator, the master. This preserves the linewidth characteristics of the master in the high power slave output. The master

oscillator in our experiment is a monolithic, single axial mode nonplanar ring oscillator pumped by a diode laser.[7]

In 1984 Kane and Byer invented the monolithic nonplanar ring oscillator (NPRO) that has several significant advantages over previously demonstrated solid-state lasers. The nonplanar ring oscillator combines the low noise of a compact monolithic design with the ability to operate in a single direction because of the built-in optical diode. To date NPRO's have operated at kilohertz free-running linewidths with noise spectral densities of $20\text{Hz}/\sqrt{\text{Hz}}$ at 1 kHz and $100\text{Hz}/\sqrt{\text{Hz}}$ at 100 Hz. This spectral density of frequency noise is three orders of magnitude below that of an Argon ion laser. The jitter linewidth of this master oscillator is typically less than 10 kHz.[8]

The lamp pumped slave laser uses a ring resonator with the Nd:YAG head from a Coherent Inc. Antares Model 76-s laser as the gain medium. The ring cavity consists of four flat mirrors and cavity stability is obtained by the thermal focussing of the Nd:YAG rod. The cavity length is 133 cm which corresponds to a free spectral range of 225 MHz. The output coupler has transmissions, $T_s = 0.17$ and $T_p = 0.45$, and 18 W of output power was obtained in a single axial mode when injection locked.

Without the master laser the slave oscillated simultaneously in both directions in 10 axial modes and with 9 watts of average power in each direction. By injection locking the slave with the output of a 40 mW master laser, the slave could be made to oscillate unidirectionally, in a single linearly polarized, TEM_{00} axial mode at the frequency of the master. When injection locked, the power in the direction of the injected light doubles to 18 W while that in the opposite direction was extinguished.

A schematic of the laser system is shown in Figure 1. The master laser is mode matched into the slave laser with a lens and is protected from the slave power, in the event that the slave looses lock and oscillates bidirectionally, by two Faraday optical isolators. Injection locking is accomplished by Pound-Drever [9] locking the slave cavity to the master frequency. The slave frequency actuation is achieved using two mirrors mounted on PZT pushers. One PZT has high dynamic range but low bandwidth and the other has high bandwidth and low dynamic range. The servo is a cascaded integrator, split into fast and slow loops, and provides 56 dB of gain at DC and has a unity gain point of 30 KHz.

The full width of the locking range [1] is given by equation 0.1 where T is the transmittance of the slave oscillator output coupler, ν_{FSR} is the slave

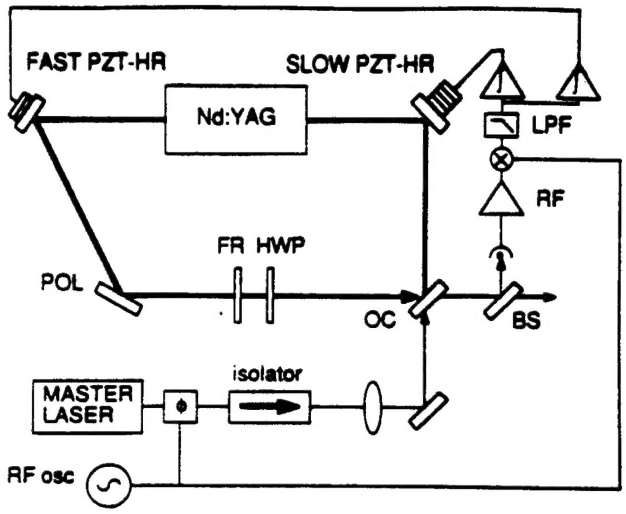

Figure 1: Injection-locked Nd:YAG Lamp pumped Antares laser system. The FM sidebands are impressed on the single-frequency, diode-laser-pumped master laser. The slave laser cavity is held at the lock point by feeding back the Pound-Drever error signal through the split servo loops to the two PZT mounted-mirrors. HR's, high reflectors; OC, output couplers; BS, beam splitter; LPF, low-pass filter.

oscillator free spectral range, and η is the spatial mode coupling efficiency factor.

$$\Delta f_{lock} = \eta \frac{T \nu_{FSR}}{\pi} \sqrt{\frac{P_{master}}{P_{slave}}} \qquad (1)$$

We measured the locking range by scanning the slave oscillator cavity length and measuring the width of the frequency discriminant from maximum to minimum of the dispersive-shaped signal. Figure 2 shows the locking bandwidth as a function of the square root of the power ratio of the master to slave. The slope of the line is 13.8 MHz which shows good agreement with the calculated value of 16.8 MHz based on $\eta = 1$. The discrepancy can be accounted for by the imperfect spatial and polarization mode overlap. We achieved injection locking with slave powers of up to 18 W with a master power of 40 mW and with about 80 percent of the power in the master carrier for a power enhancement ratio of 450.

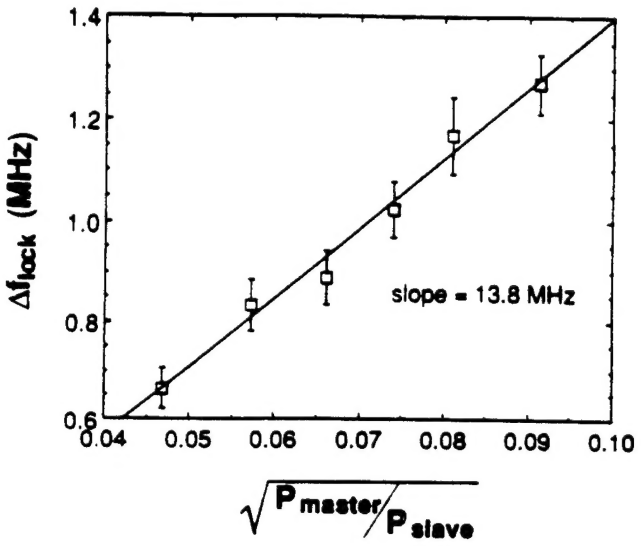

Figure 2: Injection locking range versus the square root of the ratio of the master oscillator power to the slave oscillator power. The data is fit to a straight line with a slope of 13.8 MHz.

Noise properties

There are two types of laser noise that will degrade the single-axial-mode parametric oscillator performance: frequency, and intensity noise. In the next two sections we describe our measurements of these two types of noise for the Antares laser. In addition we describe the fidelity of the Antares laser as a regenerative amplifier for the injection locking laser.

Phase fidelity of the Antares laser

To verify that the injection locked Antares slave has the same spectral purity as the NPRO master, phase fidelity measurements between the master and slave lasers were made. This measurement is made by beating a fraction of the slave laser output against a fraction of the master laser output that has been frequency shifted by 40 MHz with an acousto-optic modulator. The heterodyne beat note is then mixed down to DC to form a phase discriminator which is then analyzed using a dynamic signal analyzer.

The result of this measurement is shown in Figure 3. The measurement phase noise is well above the sensitivity limit set by residual vibration in the interferometric setup. At 1 KHz, the spectral noise density is 5×10^{-7} rad^2/Hz. The RF noise spectrum can be converted into a total phase noise spectral density $S_\phi(f)$ using

$$S_\phi(f) = \frac{2P_{ssb}(f)}{BP_c}\left(\frac{\text{radian}^2}{\text{hertz}}\right) \qquad (2)$$

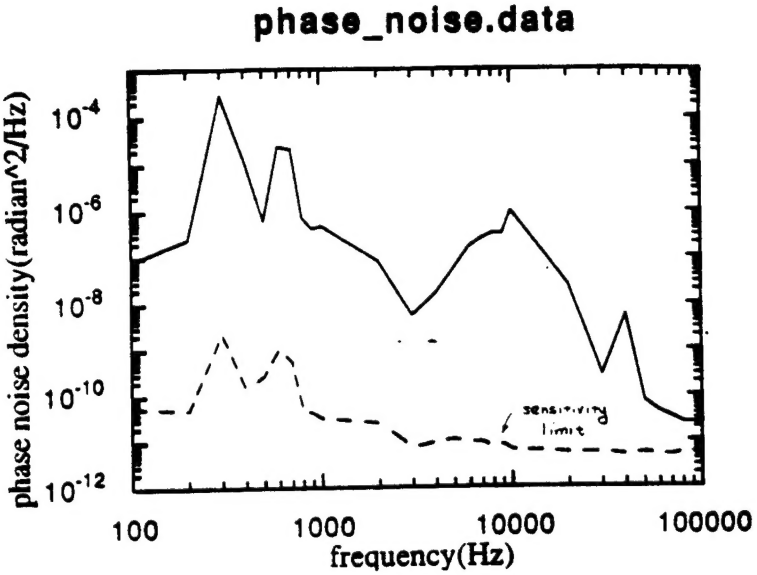

Figure 3: Phase fidelity of the regenerative slave amplifier to the master oscillator phase by the measurement of the phase noise density $S_\phi(f)$.

where $P_{ssb}(f)$ is the single sideband power density, P_c is the carrier power, and B is the resolution bandwidth. This all optical measurement yields an upper bound for $S_\phi(f)$ whereas techniques relying on the closed loop error signal yields a lower bound. By integrating the noise spectral density over the 100 KHz span, we estimate an upper bound added phase variance of 0.3 radian from the slave Antares laser. Finally, the peak at 300 Hz is due to vibration induced by water cooling inside the lamp pumped head. We expect a diode laser pumped slave laser with thermoelectric cooling to be much quieter. The additional phase noise corresponds to less than 1 kHz additional linewidth.

Frequency noise

Measurements characterizing the frequency noise spectral density of the injection locked Antares laser have been completed. Frequency noise measurements were made using the Pound/Drever [9] phase modulation discriminator while the laser was locked to a high-finesse Fabry-Perot interferometer. In these measurements, the frequency of the laser was locked to a fundamental mode of the Fabry-Perot reference cavity using a piezo to control the laser frequency. At the low end of the frequency spectrum, well within the bandwidth of the servo, the voltage on the piezo-electric tranducer provides a good representation of the frequency noise. Above the unity gain point of the servo the error signal provides a measure of the free-running frequency noise.

The Antares laser was injection locked with a 300 mW NPRO to study

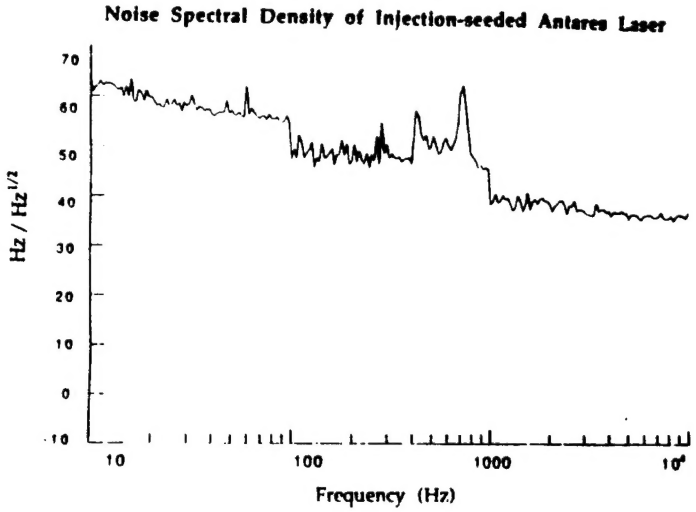

Figure 4: Free-running frequency noise of the injection locked 18 W Antares laser for a frequency range from 100 Hz to 10 kHz.

the frequency noise. The injection seed system includes servo control of the length of the slave laser (Antares) ring cavity so that it closely tracks the frequency of the master oscillator (NPRO). At low frequencies the error signal of the Antares laser is nearly identical to that of the free-running NPRO, except that there is added noise induced by the vibrations of the fan and coolant water turbulence of the Antares laser. This noise is mostly confined to the region from 400 Hz to 1 kHz.

At high frequencies the noise of the injection seeded Antares laser differs dramatically from the seed laser. The injection seeded, but free-running noise is shown in Figure 4 up to 10 kHz. The most striking difference between the noise of the injection seeded system and the NPRO alone is that there are fewer noise peaks in the slave laser spectrum than appear in the master laser spectrum. The two most significant peaks occur at 130 kHz and 260 kHz.

Overall, the noise of the injection-seeded laser closely follows the noise of the seed laser with some added noise due to mechanical vibrations. Nevertheless, the frequency noise spectral density at 1 kHz corresponds to about $50\text{Hz}/\sqrt{\text{Hz}}$ which is a factor of 50 times better than the best argon ion laser.

Intensity noise

We have measured the intensity noise spectrum of the injection-locked Antares. Measurements were made with an InGaAs PIN photodiode followed by a transimpedance amplifier and an RF spectrum analyzer. The intensity noise of the Antares, when injection locked to the 300 mW NPRO, has some peaks

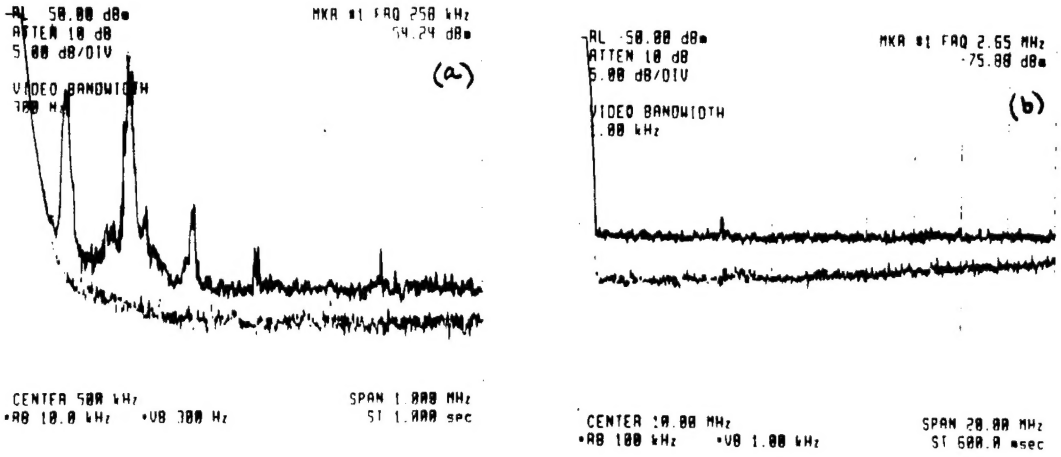

Figure 5: Intensity noise of the injection locked Antares laser (left) a frequency range from 100 Hz to 1 MHz, and a frequency range from 100 Hz to 20 MHz (right).

at integer multiples of 130 KHz as shown in Figure 5. The strongest peak is obtained at 260 KHz (70 dB above shot noise level for a resolution bandwidth of 10 KHz). These oscillations decay at higher frequency, and the intensity noise spectrum becomes shot noise limited above 5 MHz.

6.5-W, 532-nm radiation by harmonic generation

The diode-laser-pumped solid-state NPRO has proved to be an excellent source of stable, cw, single-axial-mode radiation for many applications including resonant cavity nonlinear frequency conversion. In an initial demonstration of cw harmonic conversion, Kozlovsky generated 29.6 mW of 532-nm radiation from 56-mW of 1064-nm pump radiation in a MgO:$LiNbO_3$ monolithic-external-resonant-cavity second harmonic generator.[10] The fundamental radiation was the output of a Nd:YAG NPRO pumped by a 500-mW diode-laser array. More recently we have generated 6.5 watts of cw 532-nm radiation using lithium triborate (LiB_3O_5 or LBO) in a discrete-component external-resonant-cavity harmonic generator pumped by 18 W of 1064 nm radiation.[2]

36% efficient resonant harmonic generation

The setup for the externally resonant doubling experiment is shown in Figure 6. The bow-tie cavity configuration was used to reduce astigmatism; the angle of incidence on the curved mirrors is less than 3 degrees. In addition, the ring configuration eliminates feedback into the pump laser and provides

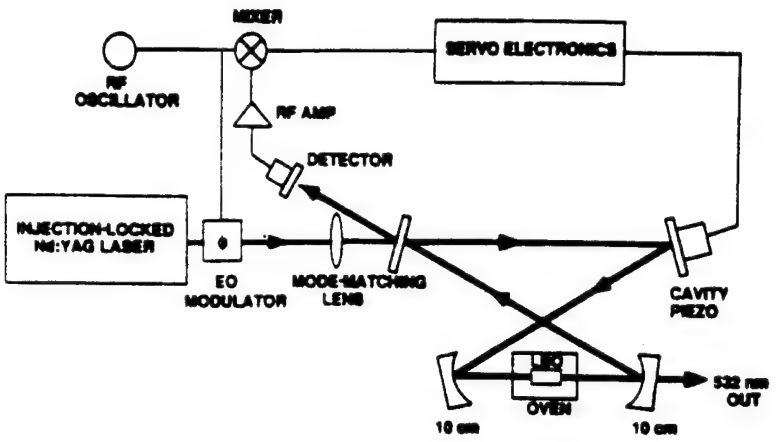

Figure 6: Experimental setup for resonant second harmonic generation. The flat mirrors in the bow tie resonator are separated by 40 cm, the curved mirrors are spaced by 10.5 cm. The laser beam is incident at 3 degrees on all mirrors.

unidirectional second harmonic output. The two curved mirrors and one flat mirror in the cavity have coatings that are highly reflecting at 1064 nm with high transmission at 532 nm. The remaining flat mirror is the input coupler which has 4.2 % transmission at 1064 nm. With this layout, a tight focal spot (1/e electric field radius) of 32 microns is formed within the nonlinear crystal, located midway between the two curved mirrors. To couple the pump laser beam into the external resonator, the external enhancement cavity resonance needs to be locked to the pump laser frequency. To maintain coincidence of the cavity resonance with the pump frequency, the cavity length is controlled with a piezoelectric-mounted mirror through a feedback loop. The feedback loop derives its error signal from the beam reflected from the input coupler using the FM sideband technique.[9]

The lithium triborate LiB_3O_5 (LBO) nonlinear crystal used in this experiment was grown at the Center for Materials Research at Stanford University. The crystal was grown from high temperature solution by the top-seeded solution growth technique. [11] Good quality boules with diameters in excess of 30 mm have been produced. LBO is well-suited for high power second harmonic generation (SHG) of Nd:YAG laser due to its high damage threshold, low absorption at both the fundamental and second harmonic, and the possibility of type I non-critical phase-matching. The 6 mm long LBO crystal was heated in an oven at 149.5°C to achieve non-critical phase matching.

The Full Width Half Maximum (FWHM) temperature bandwidth for SHG in a 1 cm length crystal is 6.8°C.

By monitoring the leakage field through one of the high reflecting mirrors of the doubling cavity, we deduced the circulating power inside the cavity and so determined the power enhancement factor. To maximize intracavity power, the external cavity must be impedance matched. Measuring losses with and without the crystal inside the cavity, we found a loss of 0.7% due to transmission and scattering of the three high reflecting mirrors. An additional 1% loss is found for transmission through the crystal. We could not determine what fraction of that 1% loss is due to the anti-reflection coatings applied to the LBO crystal and what fraction is the result of LBO bulk absorption and scattering loss. Given the 1.7% cavity round trip loss and taking into account the additional effective loss due to conversion to the second harmonic, an available mirror with transmission of 4.2% is used as the input coupler for best impedance matching. By carefully mode matching the pump laser into the resonant cavity using two 100 cm focal length lenses, 18 watts of input power yields an intracavity circulating power of 380 watts, for a fundamental power enhancement factor of 21.

Figure .7 shows the measured and predicted second harmonic power as a function of incident fundamental power and the corresponding conversion efficiency as a function of incident fundamental power. The solid line represents the theoretical fit calculated assuming an effective nonlinear coefficient of 1 pm/V for LBO, and a Boyd-Kleinman focusing parameter $h(B = 0, \xi = 0.62) = 0.58$. With a 6 mm long crystal, the calculated second harmonic conversion coefficient is 6.67×10^{-5} per watt. In calculating the theoretical fit, a correction taking into account the 90% transmission at 532 nm of the dichroic curved mirror after the crystal has been made. With this correction, the predicted and measured second harmonic power show good agreement. The maximum second harmonic power produced is 6.5 watts with 18 watts of fundamental input, representing an overall conversion efficiency of 36%. Resonant SHG is critically dependent on losses. It is reasonable to expect that with good mirrors and better crystal coatings that the round trip loss can be reduced to 0.5% and assuming perfect optical impedance matching and spatial mode matching into the external cavity, we expect a second harmonic conversion efficiency to increase from 36% to 80%.

With almost 400 watts of circulating fundamental power and 6.5-watts of second harmonic power, crystal heating caused by absorption at either

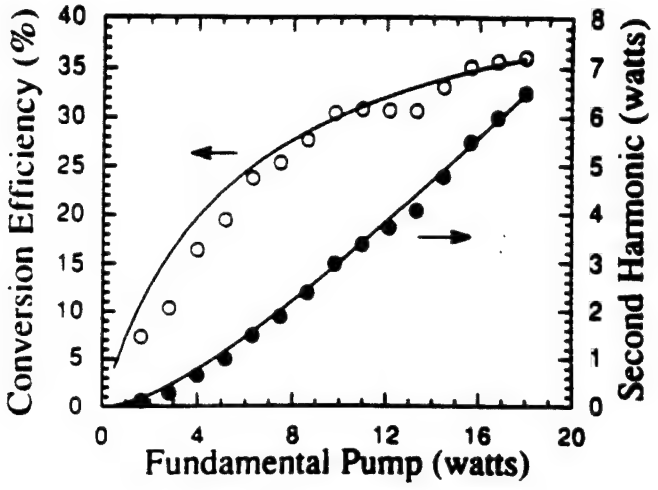

Figure 7: Resonant second harmonic generation conversion efficiency versus incident fundamental power (left axis), and the corresponding second harmonic power versus fundamental input power(right axis).

the fundamental or second harmonic wavelength becomes possible. The effect of heating on single-pass second harmonic generation efficiency has been discussed before.[12, 13] In the single pass case, heating is evidenced by a broader, asymmetric phase matching tuning curve versus temperature, accompanied by a shift in location of the peak. To assess the severity of crystal heating, we scanned the crystal oven temperature to measure phase matching tuning curve at different input pump power levels. By attenuating the fundamental input to reduce the output green power to 600 mW, we found the phase matching tuning curve to be symmetric with FWHM of 6.8°C, identical to the single pass case. At higher pump power levels resulting in 4 watts of green output, the phase matching tuning curve skews very slightly to the high temperature side, accompanied by less than 1 degree shift of the phase matching curve peak. From these observations, we conclude that heating of LBO crystal due to absorption of the fundamental or second harmonic radiation is not significant at these powers.

Spatial mode properties

The spatial mode properties of radiation to be converted in a resonant nonlinear optical device at high efficiency are very important. This is because the fundamental beam must be efficiencly mode matched into the resonant cavity and a beam with low spatial coherence cannot be efficiently coupled into the nonlinear doubling cavity. In the next two sections we discuss the

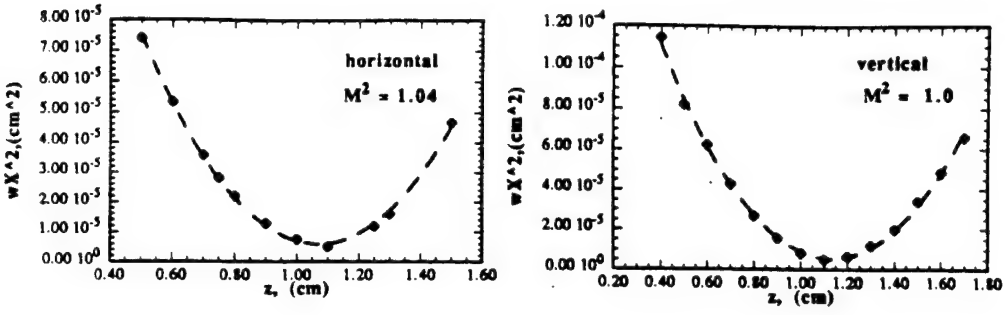

Figure 8: Antares laser spatial mode. The beam profile measured with a scanning razor blade along the horizontal x-axis (left) and vertical y-axis (right). The data are shown as dots and the fit is a gaussian profile. The beam-waist ratio beween x and y is 1.4:1.

spatial mode properties of the Antares laser and the second harmonic from the doubling cavity.

Spatial mode properties of the Antares

The transverse spatial mode structure of the slave laser determines how efficiently it can be coupled into the nonlinear frequency doubling cavity used for resonant second harmonic generation. The Antares laser output is not diffraction limited but is astigmatic due to thermal focussing. We measured the gaussian beam parameters of the beam along both orthogonal directions to the beam propagation direction.

Measurements of the transverse spatial mode profile of the Antares laser output were made using a spinning razor blade beam chopper, a photodetector and a digital oscilloscope. In Figure 8 the gaussian fit to the beam along the two axes is presented. The beam was found to be 1.7 times diffraction limited and astigmatic with a beam waist ratio between the x and y axes of 1.4:1.[1]

Spatial mode properties of the second harmonic

Figure 0.9 shows the measured green beam spatial profile and the calculated Gaussian fits. As shown in Figure 9, the beam profile along the x and y axis are essentially Gaussian with a beam waist ratio of 1:1.1 due to non-normal

[1]Subsequent adjustments to the laser optical cavity have reduced this ratio to 1.05:1.

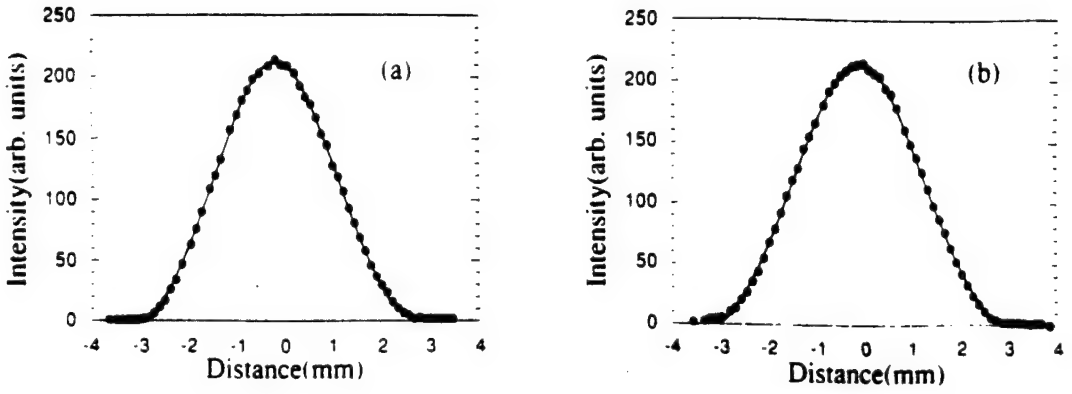

Figure 9: Measured spatial mode of the Antares laser second harmonic along (a) x-axis and (b) y-axis. Crosses represent experimental points. The solid lines are Gaussian fits. The beam waist ratio between x and y axis is 1:1.1.

incidence of the curved mirrors in the cavity. The beam quality is further characterized by measuring the spot size after focusing by a good quality doublet lens and fitting the measured spot size to Gaussian propagation formula according to Siegmans M^2 theory.[14] We determine the beam to be essentially diffraction limited with M^2 values, representing number of times diffraction limited, of 1.05 and 1.01 for the x and y axes respectively. In addition to having good spatial beam quality, the green output has excellent frequency stability. Spectral purity of the green output is confirmed by the measurements of Nabors.[15] The short-time heterodyne 3dB linewidth of 15 kHz demonstrates that the green preserves the phase fidelity of the pump laser. Aside from an initial transient when the cavity is first locked to the pump, the green output power remains within 5 percent of its starting value after one hour of continuous operation. In addition, when the external cavity lock is lost, locking is easily re-established.

We have demonstrated efficient, high-power frequency doubling, producing 6.5 watts of single frequency CW 532-nm radiation with 18-W of 1064-nm fundamental input power. The second harmonic output at 532-nm is essentially diffraction limited and inherits the frequency stability of the pump source. Such a green source is ideal as a pump for cw singly resonant parametric oscillators.

13-W diode-laser-pumped Nd:YAG laser

For the last four years work has been underway to develop a 13-W, diode-laser-pumped, solid-state laser that can reach the requirements for pumping a chirped, single-frequency, singly-resonant, parametric oscillator. This work was begun with support from ONR and SONY corp. and has for the last two years been supported by the NSF.

The most important consideration in extending diode-laser pumping of solid-state lasers to high cw output powers is efficient use of pump radiation. Collinear longitudinal pumping, otherwise known as end pumping, is a technique in which the signal and pump beams copropagate along the length of the lasing medium. This geometry uses pump radiation efficiently since the overlap between the pump and signal beams can be excellent.

End pumping suffers two limitations when extended to high power systems. First, due to the small TEM_{00} mode area in stable resonators, a very high pump brightness (in W/cm^2sr^{-1}) is required to end pump a high power laser [17]. Second, and perhaps more serious, is the thermal load on the laser medium. In any solid-state laser system, a fraction of the pump energy is dissipated as heat in the host material due to the inevitable nonradiative transitions between the pump bands and the upper fluorescence level of the laser. This thermal load leads to thermal gradients in the lasing region. Most solid-state lasers are fabricated in the shape of a long thin rod. At high pump levels this geometry suffers from thermally induced distortions such as thermal focusing, stress-induced biaxial focusing, and stress-induced birefringence. These distortions require complex correction schemes if high-efficiency, single-mode laser operation is to be achieved. The limitations of the rod geometry are well known and have led to studies of side-pumped laser systems [18].

A side-pumped laser configuration greatly reduces the pump power brightness requirement of the end-pumped system. Pumping through a large area into the lasing mode is, however, less efficient than end-pumping since the pump and signal overlap is less than perfect. In a side-pumped laser, the signal beam either passes straight through the laser medium or bounces (zigzags) off the boundaries of the medium as shown in Figure 10. The straight through geometry is still limited by thermal distortions in the laser medium. The uniformly pumped and uniformly cooled zigzag slab combines the advantages of a rectilinear geometry for reduced stress-induced birefringence and a zigzag path that eliminates thermal and stress induced focussing

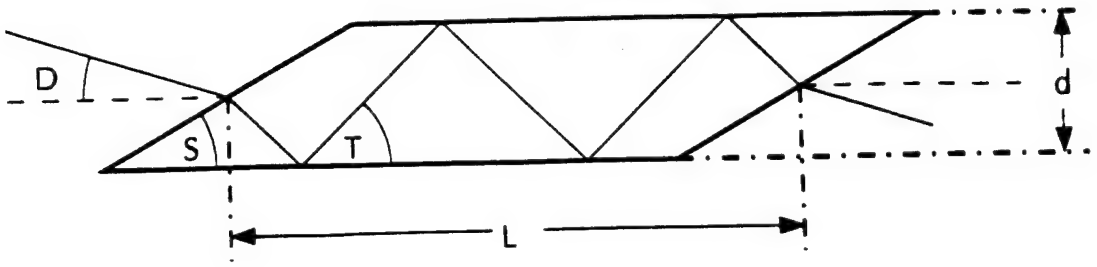

Figure 10: The geometry of the zigzag slab laser. The dimensions of the laser crystal are specified by the lengths L, d, the width of the slab (not shown), and the angle S. The optical path through the slab is determined by the incidence angle D and the bounce angle T.

[19]. The zigzag slab is a laser geometry capable of being scaled to arbitrarily high output powers.

There is no best diode-laser-pumped, solid-state laser configuration. The tradeoffs between simplicity and efficiency guarantee that the optimum design will depend on system details such as the laser material and the physical characteristics of the diode pumps. A diode pumped solid state laser able to produce 100 W of output power in a single axial mode is currently under construction for DARPA in our laboratory.

Laser design

This program has focussed on the design and the construction of a cw, single-mode, 13-watt Nd:YAG diode-laser-pumped zigzag slab laser. This laser will be pumped by 60 watts of diode laser power derived from 60 individual one-watt diode lasers as shown in figure 11. Power from the diode lasers will be coupled through optical fibers into the zigzag slab. In this subsection, we will first consider the physical dimensions of the gain medium. This discussion will be followed by a brief summary of the calculations performed to optimize the output power of the design. We will then review the laser head design, the thermal modeling calculations, and the proposed optical resonator.

The physical dimensions that describe the zigzag slab are shown in Figure 10. The equations that determine the slab dimensions are:

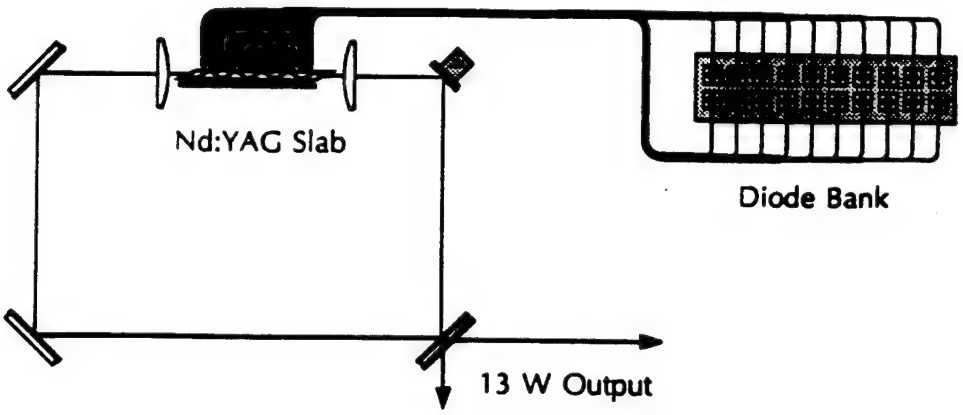

Figure 11: The 13-watt diode-laser-pumped Nd:YAG oscillator. A bank of sixty external diode lasers side pumps a zigzag slab. The gain medium is shown inside a ring resonator where cylindrical lenses are used to compensate for thermal focussing effects.

$$L = Nd \cot T, \tag{3}$$

$$\cos(s + D) = n \cos(s + T), \tag{4}$$

where N is the number of bounces in the slab and n is the index of refraction of the material. These equations guarantee that the bounces inside the slab are total internal reflections. Other constraints apply to specific slab configurations such as Brewster's angle incidence or unity fill factor. Incidence at Brewster's angle guarantees low losses for one polarization mode and imposes the following constraint on the slab dimensions

$$\tan(s + D) = \frac{1}{n}. \tag{5}$$

We chose to manufacture a collinear ($D = 0$), Brewster's angle, Nd:YAG ($n = 1.82$ at 1064nm) slab. With these constraints the slab geometry equations reduce to: $S = 28.8°$, $T = 32.4°$ and $Nd = 0.635L$. At this point we are left with one equation relating the two physical lengths of the slab to the number of bounces inside the slab. In order to minimize the scattering loss in unpumped regions of the slab, the length of the slab is chosen to be slightly greater than the size of the pump source. With L constrained in this way,

we can optimize output power by varying either the thickness of the slab or the number of bounces inside the slab.

Mathematical modeling of the output power

The operating parameters of any laser are determined by the input-output relation which can be expressed near threshold by

$$P_{out} = \left(\frac{t}{a+t} - \frac{t}{g}\right) \frac{\lambda_p}{\lambda_l} \frac{I_1^2}{I_{11}} \eta_a P_{in}, \qquad (6)$$

where P_{out} is the output power of the laser, t is the output coupling, a is the round trip loss, g is the laser gain, λ_p and λ_l are the pump and lasing wavelengths respectively, the I's are spatial overlap factors, η_a is the fraction of the pump power that leads to population inversion in the laser medium, and P_{in} is the available pump power. These parameters are related to the physical characteristics of a travelling wave laser by the following relations:

$$I_1 = \iiint_{cavity} dx\, dy\, dz s_0(x,y,z) r_0(x,y,z), \qquad (7)$$

$$I_{11} = \iiint_{cavity} dx\, dy\, dz s_0^2(x,y,z) r_0(x,y,z), \qquad (8)$$

$$g = \frac{l I_1}{I_{sat}} \eta_a P_{in}. \qquad (9)$$

In these equations, $s_0(x,y,z)$ represents the spatially dependent signal mode, $r_0(x,y,z)$ describes the spatially dependant pump mode, l is the length of the gain medium and I_{sat} is the pump saturation intensity.

Output power is maximized by choosing

$$t = t_{opt} = \sqrt{ga} - a. \qquad (10)$$

Substituting equation 0.10 into equation 0.6 leads to the optimum input-output relation

$$P_{opt} = \frac{\lambda_p}{\lambda_l} \frac{{I_1}^2}{I_{11}} \left(1 - \sqrt{\frac{a}{g}}\right)^2 \eta_a P_{in}, \qquad (11)$$

which can be analyzed in terms of four system efficiencies. The first term in Equation 11 is known as the Stokes efficiency, η_S, otherwise known as the quantum defect. This is the ultimate efficiency that any optically pumped

laser can achieve and represents the energy difference between the pump and signal photons. Obviously, the designer has no control over this parameter once the pump source and laser medium are chosen. For a diode-pumped, Nd:YAG laser pumped at 808 nm and lasing at 1064 nm, $\eta_S = 76\%$. The second term is the coupling efficiency, η_c, and depends on the pumping geometry chosen. End pumped lasers can have coupling efficiencies exceeding 80%, while 40% is typical for side pumped lasers. The third term is the laser efficiency, which is dominated by losses in the laser cavity. For example, a typical low gain laser with a 20% single pass gain has a laser efficiency of 60% at 1% loss, and 47% at 2% loss. Low loss is the most important factor leading to high-efficiency, diode-pumped lasers. The last term is the absorption efficiency, which depends mostly on the size of the gain medium relative to the absorption length of the pump. Designing a laser is an exercise in optimization. One must balance laser and absorption efficiencies, which typically improve with larger gain media, against coupling efficiency, which has the opposite tendency, all the while keeping the constraint of low losses in mind.

As we saw above, the slab geometry constrains us to vary either the thickness of the slab, or the number of bounces inside the slab. For convenience, we chose to model output power versus N. The final laser parameter that must be chosen is the TEM_{00} mode radius of the resonator cavity. Although we are free to choose this radius, there are two factors to consider: the filling factor and the aperture losses. A large beam radius fills the volume of the slab well but may be severely clipped by the slab edges. Losses are the major obstacle to efficient laser performance, so we choose a beam radius of 300 μm that suffers very little clipping while still filling a large fraction of the slab. The largest TEM_{00} mode radius practically attainable in a stable resonator is about 700 μm.

Figure 12 shows results of numerical calculations that relate coupling and absorption efficiency versus the number of bounces. We see that absorption efficiency and coupling efficiency are approximately inverses. Coupling efficiency is approximately linearly related to bounce number, indicating that the signal beam spends more time in the strongly pumped region. Absorption efficiency decreases as the bounce number increases since the slab thins with increasing bounce number. These effects combine to produce a flat output power versus N curve, which decreases at high bounce numbers due to clipping losses at the input aperture. We chose a 10 bounce slab for low

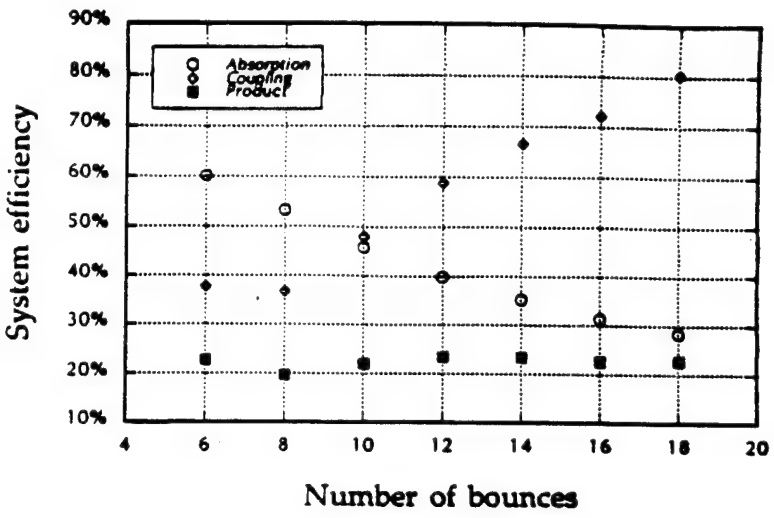

Figure 12: Variations in absorption efficiency and coupling efficiency with number of bounces. Absorption efficiency decreases due to the decreasing thickness of the slab. Coupling efficiency increases as the signal beam spends more of its time in the strongly pumped regions of the slab. The product of these two efficiencies is approximately constant with bounce number.

loss operation and to avoid a very thin design that would be difficult to manufacture. Figure 13 shows the final dimensions of the zigzag slab.

Head design

Once the dimensions of the Nd:YAG slab have been established a laser head must be designed. The laser head must perform the following functions: it must support the crystal, it must allow easy access for the pump light, it must not obstruct the signal beam, and it must allow for heat removal from the laser crystal. Traditional flashlamp-pumped rod lasers are cooled by water flowing around the rod, this system is very good at removing heat but suffers from a number of problems. The most important of these is the vibrations introduced onto the laser rod by the turbulent cooling water flow. These vibrations lead to laser frequency noise and should be avoided in order to simplify the servo requirements of the frequency stabilization system.

One of the most important advantages of diode pumping is that the significantly reduced heat load on the laser medium greatly simplifies the cooling system required. Our approach is to use thermal conduction to cool the crystal. A preliminary head design is shown in Figure .14. In this head we use the cold finger approach to cool the sides of the laser crystal, thereby allowing easy pump access. A thermoelectric cooler pulls the heat out of the assembly. Calculations show that for 25-W of heat deposited in the laser

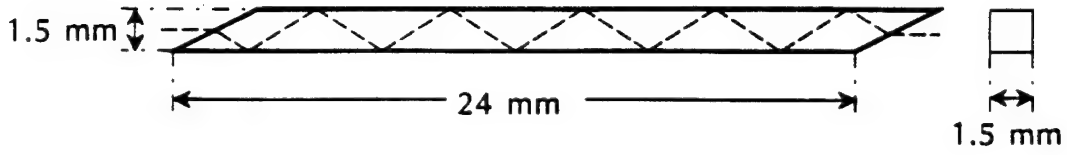

Figure 13: Final dimensions of the zigzag slab laser. The final design calls for a $1.5 \times 1.5 \times 24mm^3$ Nd:YAG slab. The optical beam will bounce off the slab walls ten times.

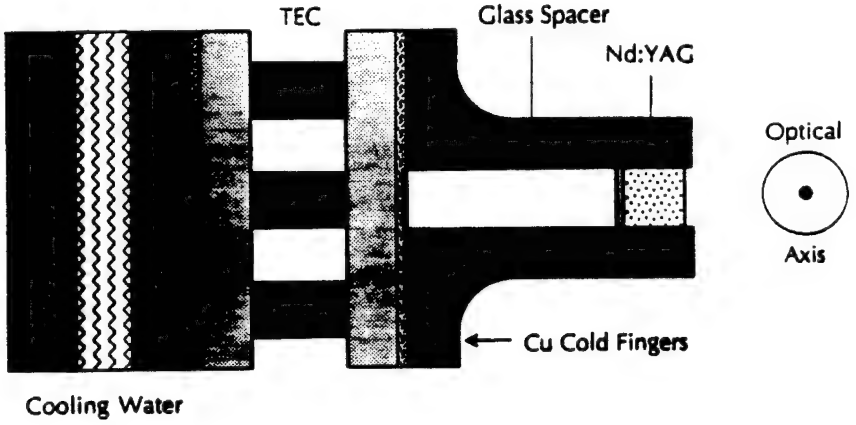

Figure 14: Preliminary laser head design. Copper cold fingers are used to cool the slab. A thermoelectric cooler pulls heat out of the assembly and deposits it in the heat sink.

crystal, a cooler current of 1.8 A is required to cool the surface of the gain medium to room temperature, assuming a heat sink temperature of 25°C. The heat sink is required to conduct 32.5-W of heat away from the laser head.

Thermal analysis

We have modeled the 13-W zig-zag slab laser using several computer programs in order to calculate the single-pass distortions of a wavefront propagating through the slab. The slab is modeled as a finite element grid with 8960 elements and 11277 nodes. The heat loading in the slab due to the pumping of the laser diodes is modeled using a Monte-Carlo ray tracing technique. Using experimentally measured values for the Nd:YAG absorption and the beam parameters of the fiber-coupled diode light, the program traces pump rays as they bounce through the slab and then computes the heat deposited in each element in the grid. These data are then used as input into a finite element analysis program which solves the steady state heat equation for the temperature distribution in the slab. A third program uses ray tracing techniques to calculate the phase distortion introduced into the laser beam due to the bulk change in the index of refraction of Nd:YAG with temperature.

We have predicted that the wavefront distortion due to the bulk temperature effects can be accurately modeled by a cylindrical lens. For example, for a heat loading of 15-W in a $1.5 \times 1.5 \times 26$ mm^3 slab, the thermal distortions is very nearly a perfect cylindrical lens of focal length 40 cm in the direction of heat removal. This thermal lensing must be taken into account when modeling the optical resonator.

We have also performed calculations on the thermally induced stress, as shown in Figure 15. The stress contours on the surface of the slab nearly follow the pumping geometry, i.e., the position of the fibers on the slab. Finally, this modelling has shown that the heat loading for this laser is less than the stress fracture limit of Nd:YAG, so that thermal management and head cooling issues are straightforward to engineer.

Optical resonator

The proposed optical resonator is a very simple, stable, four mirror design based on the resonator used in the injection-locked Antares laser system. Notable differences are the lack of an intracavity polarizer, since the Brewster's angle faces on the slab define the laser polarization. Stability is achieved by employing cylindrical lenses and the thermal focussing described above.

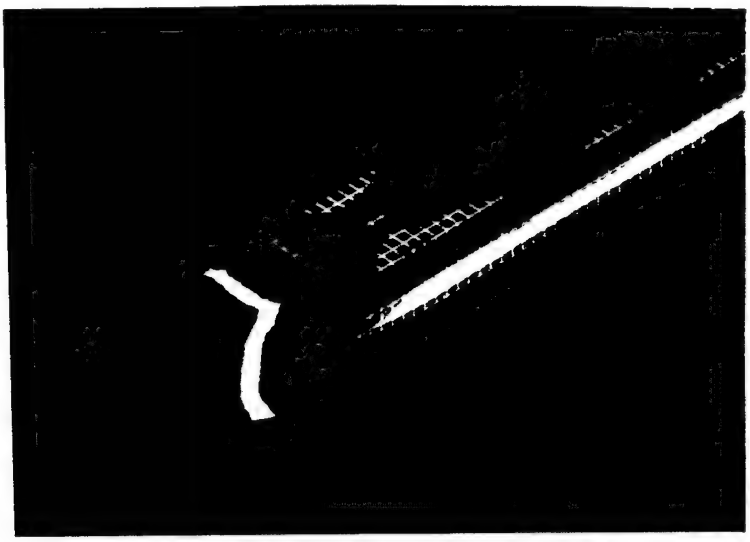

Figure 15: Surface stress resulting from the thermal loading of the 13-watt, slab laser. The bright areas show large stresses near the pump source. The calculated stresses are far below the fracture limit for the material.

Mode sizes on the order of 300 μm are expected in the gain medium.

Once we have built the laser we will investigate and compare its operation to the design theory by measuring the output power of the slab laser as a function of diode-laser-pump power, output coupling, and optical resonator design. In addition, we will measure the depolarization, the spectral density of noise, and the beam wiggle of the laser output as a function of pump power. Unidirectional oscillation and frequency stability will be achieved through injection locking rather than with intracavity etalons to keep cavity losses at a minimum and efficiency and output power high.

Diode laser pumping

An important component of any laser is the pump source. The zigzag slab laser is pumped by a bank of sixty SLU-304XRs: one-watt, fiber-coupled, diode lasers manufactured by Sony Corp. Besides the aforementioned advantages of diode pumping, fiber coupling allows the laser designer to separate the problems of cooling the laser crystal and the pump diodes. Also, the use of fiber connectors allows replacement of failed diodes while the laser is operating. These advantages come at the expense of pump brightness. Efficient (70%) coupling of a diode laser's high aspect ratio rectangular emitter to a circular core fiber typically reduces the source brightness by an order of magnitude, with a similar reduction in laser gain. This low gain laser regime demands low loss designs for efficient operation.

Diode laser drivers

Diode lasers require a highly regulated constant current source to drive them and a temperature control system to tune their output wavelength to the narrow absorption bands of Nd:YAG. In this subsection we describe the design and performance of the system used to power and cool the 1-W, diode lasers.

Our approach has been to purchase the diode laser drivers and manufacture the temperature controllers. We purchased an LDS 10000 series rack mounted laser diode driver from Light Control Instruments of San Luis Obispo, CA. These diode drivers are based on the LCI 500 series regulated current sources. Our drivers consist of two crates, each with thirty channels. Each channel is capable of driving a maximum of 4 A with a compliance of 5 V, with less than 0.05% rms noise and greater than 100 ppm/°C temperature stability. The current sources are protected by an uninterruptable power supply system to insure against premature diode failure due to spikes or blackouts in the building power.

Temperature Control

Commercially-available, high-power diode lasers are typically 20 to 40% efficient, with an emission linewidth of 2 to 5 nm. This implies that a thermal management system must be applied to remove roughly two watts of heat for every watt of optical power generated by the diode, while maintaining a junction temperature near 25°C. The junction temperature needs to be accurately controlled since the emission wavelength of diode lasers vary by 0.3 nm/°C. Given that the strong 808 nm absorption band of Nd:YAG has a linewidth of approximately 2 nm, the junction temperature needs to be controlled to better than 1°C of the setpoint. The SLU-304XR laser package includes a 10k thermistor for temperature measurement and a thermoelectric cooler for thermal management. We have calculated that the thermoelectric cooler current required to cool all sixty diode lasers to an emission wavelength of 808 nm is as follows: an average current of 790 mA per diode, and a total current of 48 A, at a diode case temperature of 5°C. This reduced case temperature greatly relaxes the current driver requirements but requires mounting the diodes on cold plates, cooled by a recirculating water chiller.

The requirements on the sixty channel temperature control system are as follows: a maximum output current of 2 A per channel, a thermistor temperature sensor input, and ±0.1°C accuracy, for negligible laser amplitude noise contributions due to pump power absorption fluctuations. Figure 0.16

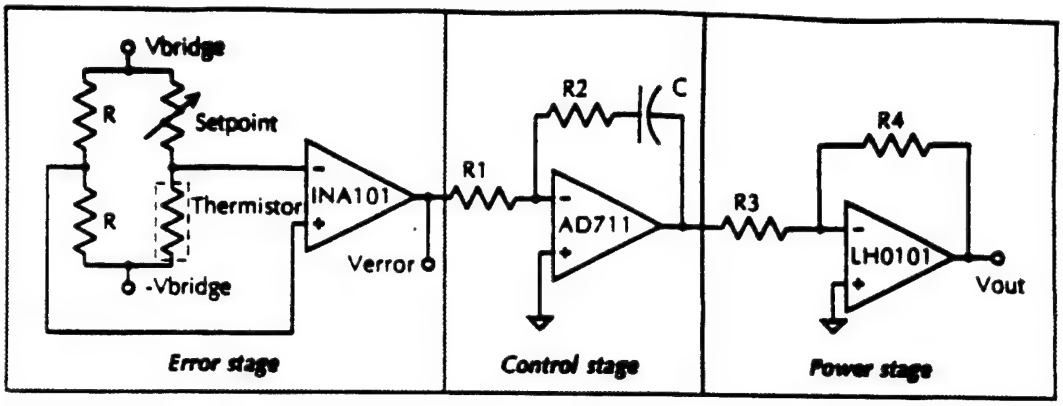

Figure 16: The design can be divided into three stages. The error stage produces a voltage proportional to temperature error. The control stage provides frequency compensation for low residual error and optimal time response. The power stage provides the drive necessary to cool the diode lasers.

shows a simple diagram of the design. The system consists of three separately optimized stages: the error stage, the control stage, and the power stage.

As shown in Figure 16, the error signal is generated by employing a balanced bridge. The precision resistor divider is used to establish a reference which is compared to the difference in resistance between the thermistor and the setpoint potentiometer. The INA101 instrumentation amplifier produces an output that has a slope of 1 V/°C for small deviations from zero error. A warning signal is generated if the error exceeds 5 V, indicating possible damage to the diode laser.

The control stage is simply a single opamp implementing a PI control law. Even with the very long time constants associated with a large thermal mass, this stage can generate large dc gain and near optimal damping ratios. The power stage consists of a single LH0101 high current amplifier, capable of delivering 5 A continuous output current while operating from a total supply voltage of 10 V. This second property is crucial in reducing power consumption.

Figure 17 shows the error signal of the temperature control unit, under actual operating conditions. The trace shows that the system achieved a diode junction temperature within 10 mC of the setpoint with peak fluctuations less than 5 mC from the mean. The sixty temperature control channels

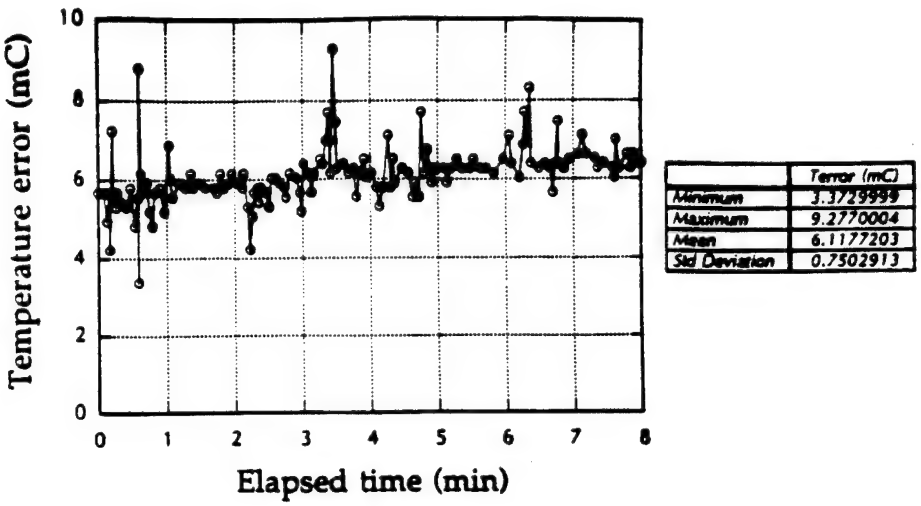

Figure 17: Temperature controller error vs time. The diode temperature is kept within 15mC of the setpoint under actual operating conditions.

are housed in three separate CAMAC crates, which provide the necessary dc power and a method of interfacing to a remote monitoring computer.

Experimental results

We have designed and built an end-pumped laser to test the laser diodes and temperature controllers in a realistic application. This laser system also provides a good way to test the predictions of the theory presented above. As shown in Figure 18, the laser consists of a single pump laser, collimation and focussing optics, a 3mm diameter by 20 mm long rod of 1.1% Nd:YAG, and an output coupler with a 1 m radius of curvature. One end of the laser rod is coated to be highly reflecting at 1064 nm and highly transmitting at 810 nm, while the other end is coated to be highly transmitting at 1064 nm.

The spatial beam parameters of the pump and signal beams were measured using a scanning razor blade chopper, and analyzed using the M^2 theory of non-diffraction limited optical beams [14]. These measurements show a beam quality factor of 100 for the fiber output beam. This large M^2 is due to the high numerical aperture fiber required for efficient diode laser coupling. Typical beam qualities for high power diode laser beams are 2 in the plane perpendicular to the diode junction and 25 in the plane parallel to the diode junction. The high M^2 values of the fiber coupled diodes dramatically show the brightness reduction that accompanies fiber coupling.

The last laser parameter that needs to be determined is the round trip loss. The theory predicts the following relationship between threshold power and output coupling

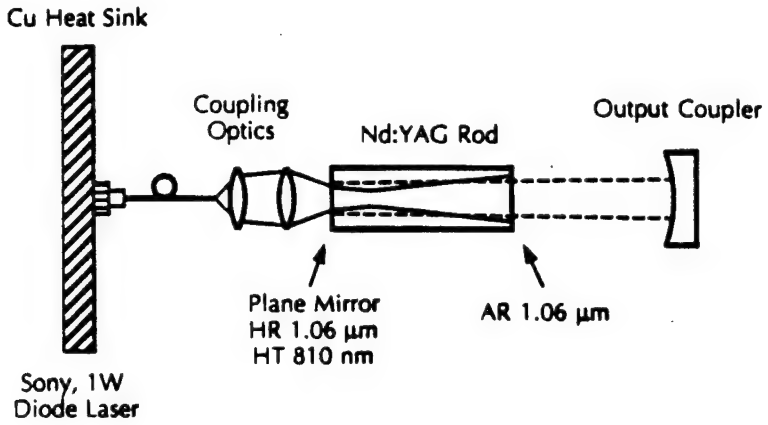

Figure 18: A schematic of the end-pumped rod laser experiment. The output of one optical fiber is focussed into the end of a coated Nd:YAG rod. A standing-wave resonator is established by the curved output coupler.

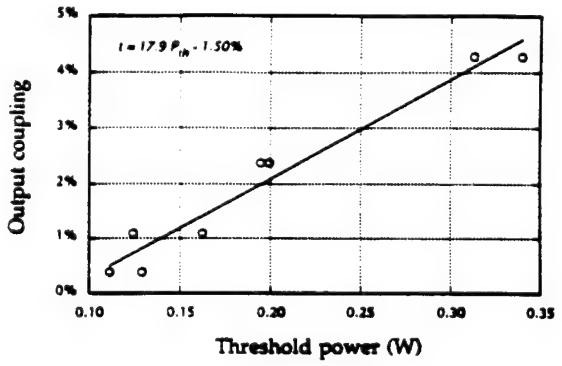

Figure 19: Findlay-Clay analysis of the rod laser. The intercept of the plot of output coupling versus threshold power yields the loss in the laser cavity, here 1.5%.

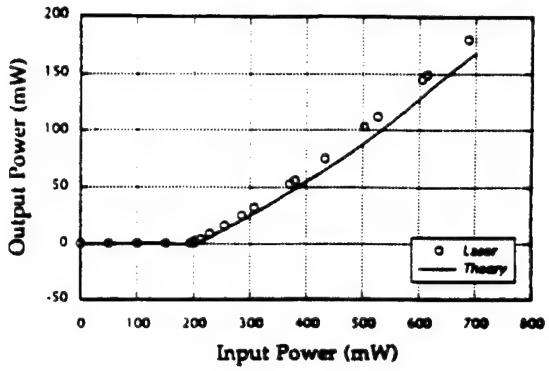

Figure 20: Input-output power graph for the rod laser. The open circles are the measured output power and the solid line is the prediction of the modelling program. The only free parameter in the calculation is used to match the predicted threshold power to that observed. The laser achieves 180mW of output power for 700 mW of pump power.

$$a + t = \frac{lI_1}{I_{sat}} \eta_a P_{th}, \tag{0.12}$$

therefore the intercept of a plot of output coupling versus threshold power yields the round trip loss in the laser. This procedure is known as the Findlay-Clay analysis [39]. The results for our laser are shown in Figure 19.

With these experimental parameters we can numerically integrate the input-output equation to predict the laser output power. The results of such a calculation are compared with experimental data in Figure 20. The predicted threshold power was close to that observed, but the theory underestimates the slope efficiency by 10%. This shows the strength of the theory in predicting the performance of diode-laser-pumped lasers.

Pulsed optical parametric oscillators

The potential of optical parametric oscillators (OPO's) for converting laser output to tunable radiation at arbitrarily selected frequencies was recognized with the first OPO demonstration.[20] The early parametric oscillators were doubly resonant. Doubly resonant oscillators (DRO's) have an advantage of low pumping threshold for oscillation, but DRO's also have complex tuning properties and stable DRO operation is difficult. These problems were

demonstrated in early experiments and analysis [20] and became more apparent with the first demonstration of continuously pumped OPO's.[21, 22] Further investigation demonstrated the stringent cavity tolerances required for stable DRO operation.[23] Theoretical analysis shows that when these tolerances are satisfied, the DRO will provide many useful and unique properties for generating tunable radiation with coherence that nearly reproduces the pump coherence.

Singly resonant optical parametric oscillators (SRO's) have less complicated tuning properties than DRO's, and SRO's are free of some of the constraints that make stable operation of DRO's difficult. Pump thresholds, however, are higher for SRO's, and it has been difficult demonstrating cw operation in these oscillators. The double resonance condition also provides frequency selectivity that easily results in single-mode-pair oscillation. This frequency selection is not available with single resonance unless frequency selecting components are added to the SRO.

SRO's have been forced to operate single-mode on the resonated signal wave even with highly multimode pumping.[24] The combined frequency selection of phase matching, a dispersing grating, and an intracavity etalon were necessary to achieve single-mode oscillation with these conditions. The multi-axial-mode pump resulted in a multimode output at the nonresonated idler field. When this type of frequency control is used with a pulsed SRO pumped with an injection-seeded Q-switched laser with single-mode output, the result is single-mode output at both the signal and idler wavelengths.[25] With the addition of piezoelectric control of the cavity length and computer control of all the adjustable parameters, spectrographic measurements with 300-MHz resolution were possible.[26] These SRO's used angle tuned $LiNbO_3$ pumped at 1.06 μm.

SRO pumped by a Q-switched laser

The single-mode pump alone is not sufficient to produce single-mode-pair oscillation in a simple SRO with no frequency selection except that of phase matching. This was observed in a BaB_2O_4 SRO pumped with the 354-nm third harmonic of the output of an injection seeded Q-switched Nd:YAG laser.[28] The single frequency pump did reduce OPO output energy fluctuation to 10% from 30% which was observed with multimode pumping when injection seeding of the Q-switched laser was blocked. The plane-parallel-cavity SRO with 1.2-cm-long BaB_2O_4 crystal and 3-cm overall length pumped by a 6-nsec pulse would oscillate on typically 8 axial modes at the signal

wave. The broad tuning range of the BaB_2O_4 OPO extending from 412 nm to 2.55 μm included both the 1.064-μm fundamental and 532-nm second harmonic of the laser, which were available for injection seeding the SRO. With injection seeding at 532 nm or 1.064 μm, the buildup time of the SRO oscillation was substantially decreased, and single-mode-pair oscillated was achieved. Measurements of the SRO threshold yielded values that were less than predicted from calculations based on reported values of the nonlinear coefficient of BaB_2O_4. This observation lead to a series of measurements that resulted in a reassessment of the scale for optical nonlinear coefficients. Injection seeding is an effective means of obtaining single-mode operation of and SRO.[29, 30, 31] A stable cw DRO would be an excellent radiation source for this application.

Long-pulse-pumped SRO's

Greater frequency selection is possible with longer buildup times of parametric oscillation. Pump pulses of 500-nsec duration were derived from a diode-pumped NPRO by gating the cw output followed by multipass amplification in a flashlamp pumped laser amplifier.[32] A monolithic SRO was pumped by the second harmonic generated by the oscillator-amplifier laser system. Pumping with the 532-nm harmonic allowed noncritical phase matching in the 5%MgO:$LiNbO_3$ crystal. The purpose of this experiment was to investigate spectral narrowing and to reduce OPO threshold to a level approaching that which could be achieved directly by diode-pumped lasers.

The monolithic SRO tuned from 834 to 958 nm and 1.47 to 1.2 μm when temperature was adjusted between 190° and 125°C.[3] Damage limitation of the MgO:$LiNbO_3$ SHG crystal required that the 5-kW output of the laser amplifier be no longer than 500 ns. Under these conditions 800 W of 532-nm harmonic was generated. The ring-cavity configuration of the SRO allowed high efficiency; up to 60% pump depletion was observed after threshold was reached. About 20% of the time single-mode operation of the SRO was observed. More often, however, simultaneous oscillation on three axial modes was observed, and occasionally as many as 8 modes oscillated simultaneously. Thus long-buildup time alone was not sufficient to guarantee single-mode oscillation.

Pulse-pumped doubly resonant optical parametric oscillation A further reduction in OPO threshold is obtained with the doubly resonant oscillator (DRO) configuration in which the OPO is resonant at both the signal and idler wavelengths. The added constraint of double resonance in addition

to phase matching and conservation of energy, however, makes stable operation of the DRO difficult.[3] The frequency stability of the NPRO and the mechanical stability of monolithic DRO construction are useful in overcoming this difficulty. A doubly resonant monolithic DRO was constructed from MgO:$LiNbO_3$ with broad-band dielectric mirrors highly reflecting near 1.06 μm coated on the crystal.[33] A ring geometry was formed by using reflections from two 10-mm radius-of curvature surfaces on the ends of the noncritically phase-matched, 1.25-cm-long crystal and a polished flat on one side for total internal reflection (Figure 21). The DRO was pumped at 532 nm by second-harmonic pulses generated from the relaxation oscillations of a Nd:YAG NPRO. Pulsed operation was required because the DRO threshold was marginally higher than could be produced by the NPRO and harmonic generator when operated cw.

A 10% modulation of the diode-laser current at 325 kHz drove the Nd:YAG NPRO into relaxation oscillations. The 1.06-μm fundamental pulses had 260-mW peak power and were efficiently converted into 400-ns, 230-mW, 532-nm pulses by externally resonant second-harmonic generation. The buildup of parametric oscillation occupied most of the pump pulse duration. Overall DRO efficiency was only 7% due to the long buildup time. After threshold was reached 60% pump depletion occurred. The DRO tuned between 1.02 and 1.12 μm by adjustment of both temperature and electric field. The most remarkable aspect of the DRO operation was that single-mode-pair oscillation was achieved on almost every pulse. The only exception was when the DRO was tuned between cluster centers and either simultaneous or alternating output on widely spaced modes approximately 4 nm apart were observed. The monolithic DRO with a pulsed single-mode pump will oscillate on a single mode pair due to the constraint of double cavity resonance.

CW optical parametric oscillators

Our cw OPO experiments have used the second harmonic radiation described above for pumping. The availability of 532-nm pump radiation and noncritical phase matching with a reasonable temperature tuning range in MgO:$LiNbO_3$ was important for these experiments. Temperature-tuned noncritically phase-matched monolithic resonators provided mechanical stability and low loss for these DRO studies. A drawing of a ring-path monolithic OPO is shown in Figure 21. Pulsed radiation of 400-ns duration and cw 532-nm radiation produced by the monolithic resonant cavity harmonic generator was

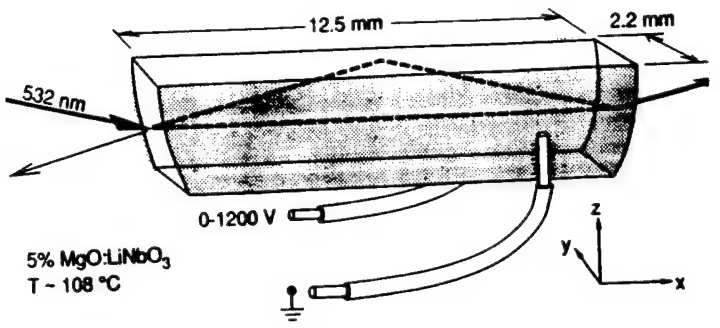

Figure 21: Monolithic DRO geometry used for experimental observations

used to pump the DRO's.[34] The DRO performance was remarkable. The threshold for the cw device was only 11 mW. Single-mode-pair output was observed routinely in the cw DRO's. As much as 80% pump depletion was observed at two times above threshold.The output coupling of the OPO was not optimized for maximum output. Nevertheless, the slope efficiency shown in Figure 22 was 64% and surprisingly linear. The free-running cw DRO without servo control would oscillate for periods of one minute on a single mode pair. At degeneracy the DRO would stably produce the subharmonic of the pump for periods of 20 minutes.

The coherence properties of the cw DRO are also remarkable.[15] It was observed during the periods of stable operation between mode hops that the coherence of the outputs of the DRO reproduced the coherence of the pump radiation. When operated on a mode pair adjacent to degeneracy, the signal and the idler difference frequency was stable to better than 1 kHz, the limit of resolution of the measurement. The difference frequency of the signal and the idler is an indication of the additional frequency noise that the DRO adds to that present on the pump radiation. At degeneracy, the output of the DRO was a phase-locked subharmonic of the pump radiation. This was shown by interference of the DRO output and the laser radiation used to generate the second harmonic that was in turn used to pump the DRO.

Our measurements of DRO performance and coherence provided the basis for a theoretical analysis of the frequency-tuning and -control properties of these devices.[35] The analysis showed how three tuning parameters are required for controlling two cavity resonances and phase matching in the

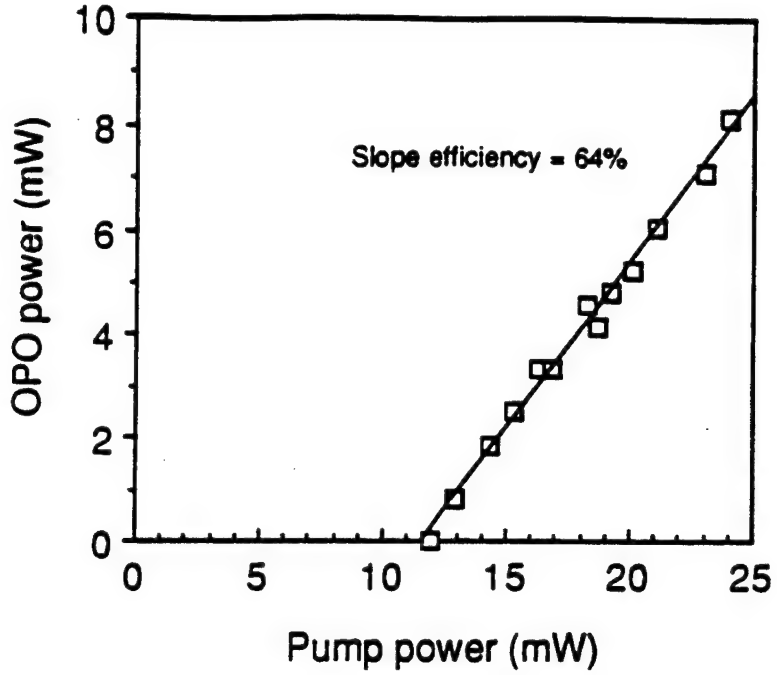

Figure 22: Output power as a function of pump power for a cw monolithic $MgO:LiNbO_3$ DRO. The DRO was pumped at 532 nm and the output was near degeneracy at 1.064 μm.

DRO. It was possible to model the observed tuning properties of monolithic $MgO:LiNbO_3$ DRO's using temperature dependent dispersion, thermal expansion, electro-optic, and piezoelectric properties of the material. The analysis is applicable to both monolithic and discrete component cavities. The tuning analysis can be used to calculate the tolerances for stable DRO operation. These tolerances are stringent, for example 0.001°C temperature stability and 5×10^{-10} m cavity length stability are typical requirements. More stringent tolerances than these, however, are achieved in laser frequency stabilization. Lasers are now available that provide the required frequency stability for resonant cavity nonlinear frequency conversion techniques. It is an interesting and important challenge to reproduce the available laser frequency stability in the output of a nonlinear frequency conversion device.

Publications resulting from this program

The publications resulting from the Office of Naval Research contract ONR N00014-88-K-0701, "An All-Solid-State Chirped Source for Coherent Optical Radar". Reprints of these publications are contained in the Appendix.

W. J. Kozlovsky, E. K. Gustafson, R. C. Eckardt and R. L. Byer, "Efficient monoolithic MgO:$LiNbO_3$ singly resonant optical parametric oscillator," Opt. Lett. 13, 1102 (1988).

R. L. Byer, "Frequency stable high power lasers in space," Relativistic Gravitational Experiments in Space, edited by R. W. Hellings (NASA Headquarters, Washington, D.C, 1989), pp. 166-170.

M. K. Reed and R. L. Byer, "Mode-locked operation af a Nd:YLF laser and amplification in a Q-switched Nd:glass slab laser," IEEE J. Quantum Electron. 26, pp. 1399-1404 (1990).

C. D. Nabors and R. L. Byer, "Monolithic Optical Parametric Oscillators for Quantum Optics," Coherence and Quantum Optics VI, edited by J. H. Eberly, L. Mandel and E. Wolf (Plenum, New York, 1990), pp. 787-791.

C. D. Nabors and R. M. Shelby, "Two-color squeezing and sub-shot-noise signal recovery in doubly resonant optical parametric oscillators," Phys. Rev. 42, pp. 556-559 (1990).

C. D. Nabors, S. T. Yang, T. Day and R. L. Byer, "Coherence properties of a doubly-resonant monolithic optical parametric oscillator," J. Opt. Soc. Am. B 7, pp. 815-820 (1990).

M. K.Reed and R. L. Byer, "The output beam quality of a Q-switched Nd:Glass slab laser," IEEE J. Quantum Electron. 26, pp. 2138-2145 (1990).

R. C. Eckardt, C. D. Nabors, W. J. Kozlovsky and R. L. Byer, "Optical parametric oscillator frequency tuning and control," J. Opt. Soc. Am B 8, pp. 646-667 (1991).

R. C. Eckardt, H. Masuda, Y. X. Fan and R. L. Byer, "Absolute and rela-

tive nonlinear optical coefficients of KDP, KD*P, BaB2O4, LiIO3, MgO:LiNbO3, and KTP measured by phase-matched second harmonic generation," IEEE J. Quantum Electron. 26, pp. 922-933 (1990).

T. Day, E. K. Gustafson and R. L. Byer, "Active frequency stabilization of diode laser pumped, nonplanar ring oscillators," Proc. SPIE 1223, pp. 181-185 (1990).

T. Day, A. D. Farinas and R. L. Byer, "Demonstration of a low bandwidth 1.06 m optical phase-locked loop for coherent homodyne communication," IEEE Photonics Tech. Lett. 2, pp. 294-296 (1990).

S.T. Yang, C.C. Pohalski, E.K. Gustafson, R.L. Byer, R.S. Feigelson, R.J. Raymaker, and R.K. Route,"6.5-W, 532-nm radiation by cw resonant external-cavity second-harmonic generation of an 18-W Nd:YAG laser in LiB_3O_5," Optics Letters, Vol. 16, No. 19, October 1, 1991, 1493-1495.

R. L. Byer, "Advances in nonlinear optical materials and devices," to be published in Proceedings of the 5th Toyota Conference on Nonlinear Optical Materials, Aichi-ken, Japan, 6-9 October 1991, S. Miyata, ed. (Elsevier Science, Amsterdam, 1992).

T. Day, E. K. Gustafson and R. L. Byer, "Sub-Hertz frequency stabilization of two diode-laser pumped-Nd:YAG lasers locked to a Fabry-Perot interferometer," submitted to J. of Quantum Electronics.

R. C. Eckardt, T. Day, E. K. Gustafson and R. L. Byer, "Frequency stable operation of Nd:YAG Lasers," to be published, Proceedings of the 5th International School on Laser Applications in Atomic, Molecular and Nuclear Physics, (Vilnius University Press, Vilnius, Lithuania).

Dissertations resulting from this program

The dissertations resulting from the Office of Naval Research contract ONR N00014-88-K-0701, "An All-Solid-State Chirped Source for Coherent Optical Radar".

W.J. Kozlovsky, "Efficient nonlinear conversion of frequency-stable lasers," Department of Applied Physics, Stanford University, November 1988.

C.D. Nabors, "Coherence and two-color squeezing in doubly resonant parametric oscillators," Department of Applied Physics, Stanford University, December 1989.

A.C. Nilsson, "Eigenpolarization theory and experimental linewidth study of monolithic nonplanar ring oscillators," Ph.D. dissertation, Dept. of Applied Physics, Stanford University, Stanford California, 1989.

M. K. Reed, "Nd:Glass slab laser development and applications for x-ray lithography," Department of Applied Physics, Stanford University, June 1990.

T. Day, "Frequency stabilized solid state lasers for coherent optical communications," Dept. of Electrical Engineering, Stanford University, Stanford California, 1990.

R.C. Eckardt, "Continuous tuning and frequency stabilization of doubly resonant optical parametric oscillators," Department of Applied Physics, Stanford University, June 1991

Personnel supported by this program

The personnel supported by the Office of Naval Research contract ONR N00014-88-K-0701, "An All-Solid-State Chirped Source for Coherent Optical Radar".

Professor Robert L. Byer
Professor Martin M. Fejer
Senior Research Associate Robert Eckardt
Research Associate Eric Gustafson
Graduate Student Alex Farinas
Graduate Student Steven Yang
Graduate Student Chris Pohalski
Graduate Student Stephan Schiller
Graduate Student David Nabors
Graduate Student Murray Read
Graduate Student William J. Kozlovsky

Conclusion

We have reported on progress under the Office of Naval Research contract ONR N00014-88-K-0701, "An All-Solid-State Chirped Source for Coherent Optical Radar". This progress includes seven principle accomplishments including: the demonstration of an 18-watt, single-frequency, injection-locked, TEM_{00}, Nd:YAG laser, the measurement of the phase fidelity of this regenerative amplifier and the frequency, and intensity noise of the injection locked laser, the conversion of the output of this laser to 6.5 watts of single-frequency, TEM_{00}, green radiation at 532 nm by resonant second harmonic generation, the measurement of the spatial mode characteristics of this lasers and its second harmonic, the progress toward a 13-watt, single-frequency, diode-laser-pumped, solid-state laser, the construction and testing of a pulsed parametric oscillator, and the construction of a cw doubly resonant parametric oscillator and the use of this 80% efficient device for the generation of squeezed states.

References

[1] C.D. Nabors, A.D. Farinas, T. Day, S.T. Yang, E.K. Gustafson and R.L. Byer,"Injection locking of a 13-W cw Nd:YAG ring laser", Opt. Lett. 14, pp. 1189-1191 (1989).

[2] S.T. Yang, C.C. Pohalski, E.K. Gustafson, R.L. Byer, R.S. Feigelson, R.J. Raymaker, and R.K. Route,"6.5-W, 532-nm radiation by cw resonant external-cavity second-harmonic generation of an 18-W Nd:YAG laser in LiB_3O_5", Optics Letters, Vol. 16, No. 19, October 1, 1991, 1493-1495.

[3] W. J. Kozlovsky, E. K. Gustafson, R. C. Eckardt and R. L. Byer, "Efficient monolithic MgO:$LiNbO_3$ singly resonant optical parametric oscillator," Opt. Lett. 13, 1102 (1988).

[4] C.D. Nabors, R.M. Shelby,"Two-color squeezing and sub-shot-noise signal recovery in doubly resonant optical parametric oscillators," Phys. Rev. A, 42, 556-559 (1990).

[5] T. Day, E.K. Gustafson and R.L. Byer,"Sub-Hertz frequency stabilization of two diode laser pumped Nd:YAG lasers locked to a Fabry-Perot interferometer," To be published in the special issue of the Journal of Quantum Electronics in March 1992.

[6] R. Adler, Proc. IRE 34, 351 (1946).

[7] T.J. Kane and R.L. Byer, "Monolithic unidirectional single-mode Nd:YAG ring laser", Optics Letters, vol. 10, pp. 65-67, (1985).

[8] T.J. Kane, A.C. Nilsson, and R.L. Byer, "Frequency stability and offset locking of a laser-diode-pumped Nd:YAG monolithic nonplanar ring oscillator," Opt. Lett., 12, 175-177 (1987).

[9] R.W.P. Drever, J.L. Hall, F.V. Kowalski, J. Hough, G.M. Ford, A.J. Munley, and H. Ward, "Laser Phase and Frequency Stabilization using an Optical Resonator," Appl. Phys. B 31, 97-105 (1983).

[10] W. J. Kozlovsky, C. D. Nabors and R. L. Byer, IEEE J. Quantum Electron. 24, 913 (1988).

[11] R.S. Feigelson and R.K. Route, Proc. Eighth American Conference on Crystal Growth, pp. 123b, Vail, Colorado, July 1990.

[12] M. Okada, S. Ieiri, IEEE J. Quantum Electron. QE-7, pp. 469-470 (1971).

[13] M. Okada, S. Ieiri, IEEE J. Quantum Electron. QE-7, pp. 560-563 (1971).

[14] Anthony E. Siegman, Lasers, Ch. 11, (Mill Valley: University Science Books, 1986).

[15] C.D. Nabors, S.T. Yang, T. Day and R.L. Byer, "Coherence properties of a doubly resonant monolithic optical parametric oscillator," J. Opt. Soc. Am. B, Vol 7, No. 5, May 1990, pp. 815-820.

[16] K. Kubodera and K. Otsuka, "Single-Transverse-Mode $LiNbP_4O_{12}$ Slab Waveguide Laser," J. Appl. Phys 50 (2) Feb. 1979

[17] T.Y. Fan and A. Sanchez, "Pump source requirements for end-pumped lasers," IEEE Journal of Quantum Electronics, Vol. 26, No. 2, February 1990, pp.311-316.

[18] J.M. Eggelston, T.J. Kane, K. Kuhn, J. Unternahrer, and R.L. Byer, "The slab geometry laser-Part I: Theory," IEEE J. Quant. Electron. QE-20, 289 (1984).

[19] W.S. Martin and J.P. Chernoch, "Multiple Internal Reflection Face Pumped Laser," US Patent 3633 126, 1972.

[20] J. A. Giordmaine and R. C. Miller, in Physics of Quantum Electronics,P. L. Kelly, B. Lax and P. E. Tannenwald, eds. (McGraw, New York, 1965), pp. 31-42.

[21] R. G. Smith, J. E. Geusic, H. J. Levinstein, J. J. Rubin, S. Singh and L. G. Van Uitert, Appl. Phys. Lett. 12, 308 (1968).

[22] R. L. Byer, M. K. Oshman, J. F. Young and S. E. Harris, Appl. Phys. Lett. 13, 109 (1968).

[23] R. G. Smith, IEEE J. Quantum Electron. QE-9, 530 (1973).

[24] S. J. Brosnan and R. L. Byer, IEEE J. Quantum Electron. QE-15, 415 (1979).

[25] T. K. Minton, S. A. Reid, H. L. Kim and J. D. McDonald, Opt. Commun. 69, 289 (1989).

[26] T. K. Minton, H. L. Kim, S. A. Reid and J. D. McDonald, J. Chem. Phys. 89, 6550 (1988).

[27] Y. X. Fan, R. C. Eckardt, R. L. Byer, J. Nolting and R. Wallenstein, Appl. Phys. Lett. 53, 2014 (1988).

[28] T.Y. Fan and R.L. Byer, "Diode-laser-pumped solid-state lasers," IEEE J. Quant. Electron. QE-24, 6 (1988)

[29] J. E. Bjorkholm and H. G. Danielmeyer, Appl. Phys. Lett. 15, 171 (1969).

[30] V. L. Boichenko, M. M. Novikov and A. I. Kholodnykh, Sov. J. Quantum Electron. 17, 392 (1987).

[31] J. G. Haub, M. J. Johnson, B. J. Orr and R. Wallenstein, Appl. Phys. Lett. 58, 1718 (1991).

[32] T. J. Kane, W. J. Kozlovsky and R. L. Byer, Opt. Lett. 11, 216 (1986).

[33] W. J. Kozlovsky, C. D. Nabors, R. C. Eckardt and R. L. Byer, Opt. Lett. 14, 66 (1989).

[34] C. D. Nabors, R. C. Eckardt, W. J. Kozlovsky and R. L. Byer, Opt. Lett. 14, 1134 (1989).

[35] R. C. Eckardt, C. D. Nabors, W. J. Kozlovsky and R. L. Byer, J. Opt. Soc. Am. B 8, 646 (1991).

[36] R.L. Byer,"Diode laser-pumped solid-state lasers," Science, 239,742-747 (1988).

[37] W.J. Kozlovsky, C.D. Nabors and R.L. Byer,"Efficient second harmonic generation of a diode-laser-pumped cw Nd:YAG laser using monolithic MgO:$LiNbO_3$ external resonant cavities," IEEE J. Quantum Electron. QE-24, pp. 913-919 (1988).

[38] D.H. Jundt, M.M. Fejer, R.L. Byer, R.G. Norwood, and P.F. Bordui, "69% Efficient continuous-wave second-harmonic generation in lithium-rich lithium niobate," Opt. Lett, Vol. 16, No. 23, December 1, 1991, pp.1856-1858.

[39] D. Findlay and R.A. Clay,"The measurement of internal losses in 4-level lasers," Physics Letters, Volume 20, number 3, 15 February 1966, pp.277-278.

[40] A.C. Nilsson, "Eigenpolarization theory and experimental linewidth study of monolithic nonplanar ring oscillators," Ph.D. dissertation, Dept. of Applied Physics, Stanford University, Stanford California, 1989.

[41] A.C. Nilsson, E.K. Gustafson, and R.L. Byer, "Eigenpolarization theory of monolithic nonplanar ring oscillators," J. Quantum Elec., 25, April 1989, pp.767-790.

[42] W.J. Kozlovsky, C.D. Nabors and R.L. Byer, "Second-harmonic generation of a continuous-wave diode-pumped Nd:YAG laser using an external resonant cavity," Opt Lett 12, 12 (1987), pg. 1014

[43] W.J. Kozlovsky "Efficient Resonant Harmonic Generation of a Nd:YAG Laser," Dissertation, Stanford University December 1988

[44] W.J. Kozlovsky, C.D. Nabors, R.C. Eckardt, and R.L. Byer,"Monolithic MgO:$LiNbO_3$ doubly resonant optical parametric oscillator pumped by

a frequency-doubled diode-laser-pumped Nd:YAG laser," Opt. Lett., 14, 66-68 (1989).

[45] W.J. Kozlovsky, C.D. Nabors, and R.L. Byer,"Efficient second harmonic generation of a diode-laser-pumped CW Nd:YAG laser using monolithic MgO:LiNbO3 external resonant cavities," IEEE J. Quantum Electron., Vol. 24, No. 6, June (1988) pp. 913-919.

[46] C.D. Nabors, W.J. Kozlovsky, and R.L. Byer, "Efficient second harmonic generation of a diode-pumped cw Nd:YAG laser using an externally resonant cavity," SPIE (1988).

[47] M.K. Reed, R.L. Byer,"Performance of a conduction cooled Nd:Glass slab laser," SPIE 736 (1987).

[48] M.K. Reed, W.J. Kozlovsky, R.L. Byer, G.L. Harnagel and P.S. Cross, "Diode Laser Array Pumped Nd:YAG and Nd:Glass Laser Source," post deadline paper, Topical Meeting on Coherent Laser Radar: Technology and Applications, Aspen, Colorado, July 27-31, 1987.

[49] M.K. Reed, W.J. Kozlovsky , R.L. Byer, G.L. Harnagel, and P.S. Cross, "Diode Laser Array Pumped Nd:YAG and Nd:Glass Slab Oscillators,"Opt. Lett., 13, 204-206, March, 1988.